# Vortex phase diagram of $Ba(Fe_{0.93}Co_{0.07})_2As_2$ single crystals

R. Prozorov,* N. Ni, M. A. Tanatar, V. G. Kogan, R. T. Gordon, C. Martin, E. C. Blomberg, P. Prommapan, J. Q. Yan, S. L. Bud'ko, and P. C. Canfield

*Ames Laboratory and Department of Physics & Astronomy, Iowa State University, Ames, Iowa 50011, USA*

(Received 7 October 2008; published 4 December 2008)

Irreversible magnetic properties of $Ba(Fe_{0.93}Co_{0.07})_2As_2$ single crystals were studied by using several techniques including transport, magnetization, and magneto-optics. The mixed-state response was found to be very similar to high-$T_c$ cuprates, such as Y-Ba-Cu-O and Nd-Ce-Cu-O. In particular, we find a nonmonotonic "fishtail" shape of the magnetization loops $M(T=\text{const},H)$ and a corresponding feature in $M(T,H=\text{const})$ scans, as well as a very large magnetic relaxation rate. The supercurrent density, $j$, in the critical state was evaluated from magnetization and from direct transport measurements close to $T_c$. At 5 K we estimate a moderate $j \approx 2.6 \pm 0.2 \times 10^5$ A/cm$^2$. Analysis of the temperature and field dependencies of the magnetic relaxation is consistent with the collective pinning and creep (weak pinning and fast creep) model and suggests a crossover from the collective to the plastic creep regime in fields exceeding the field at which the fishtail magnetization is maximum. While the zero-field anisotropy of the magnetic properties in the superconducting state of $Ba(Fe_{0.93}Co_{0.07})_2As_2$ is small, the vortex behavior changes for different orientations of magnetic field with respect to the crystal axes, implying field-dependent anisotropy of pinning properties.

DOI: 10.1103/PhysRevB.78.224506 PACS number(s): 74.25.Sv, 74.25.Ha, 74.25.Qt, 74.25.Dw

## I. INTRODUCTION

The recently discovered iron-based pnictides are layered materials with superconductivity presumably residing in the Fe-As layers. This feature, also present in high-$T_c$ cuprates, may suggest that this new class of materials could have similarly rich static and dynamic properties in the mixed state when Abrikosov vortices are present. So far, only a limited amount of information on the vortex behavior in single crystals of Fe-based pnictides is available. In polycrystalline samples, the magnetic behavior is significantly affected by the extrinsic factors such as grain morphology, surface roughness, and intergrain voids and interfaces. Some of the grains are not even superconducting.[1] Still, important properties such as upper critical fields, electromagnetic granularity, and the peak effect were studied in polycrystalline samples, and these studies hinted at some similarities in the vortex behavior between pnictides and cuprate superconductors.[2–4]

This similarity was clearly revealed in the measurements of magnetization and magnetic relaxation in individual single crystals of the oxypnictide superconductor $NdFeAsO_{1-x}F_x$, in particular the existence of a large magnetic relaxation rate and relatively weak pinning.[1] Later torque measurements on the similar Sm-based system have lead to the conclusion that the anisotropy of the magnetic properties in the superconducting state is large and quite temperature dependent.[5] More recent high-field torque measurements on similar crystals have shown a much smaller anisotropy.[6]

The superconducting crystals based on the parent RFeAsO compound (1111 system, where R is a rare-earth element) are small and difficult to study. On the other hand, large crystals based on the related oxygen-free parent compound $AFe_2As_2$ (122 system, where A is an alkaline-earth element) can be grown in flux at ambient pressure [see, e.g., $A$=Ba,[7] Sr,[8] and Ca (Ref. 9)]. Both the A and Fe sites can be doped to achieve superconductivity with holes or electrons as carriers, respectively. For example, among other results, detailed thermodynamic measurements of the $Ba_{1-x}K_xFe_2As_2$ compound have shown a very low anisotropy of the second critical field, ~3 (Refs. 7 and 10). The work performed on superconducting $Ba(Fe_{1-x}Co_x)As_2$ has shown that Co doping does not introduce a significant amount of additional scattering.[11] The fishtail magnetization and anisotropy in 122 single crystals have been reported in Refs. 12 and 13. High-field properties,[14] as well as penetration depth studies[15] of single crystals of this compound are reported elsewhere. It is this system that we have chosen for the present study due to its superior superconducting properties.

In this paper we use global and local magnetization data, as well as transport measurements to study the vortex pinning and magnetic relaxation, to evaluate the critical state supercurrents and to construct the mixed-state phase diagram for single crystals of $Ba(Fe_{0.93}Co_{0.07})_2As_2$.

## II. EXPERIMENT

Single crystals of $Ba(Fe_{0.93}Co_{0.07})_2As_2$ were grown out of FeAs flux using high-temperature solution growth techniques. The powders of FeAs and CoAs were mixed with Ba in the ratio Ba:FeAs:CoAs=1:3.6:0.4. The mixture was placed into an aluminum crucible and a second catch crucible containing quartz wool was placed on top of the growth crucible. Both were sealed in a quartz tube under argon and slowly heated to 1180 °C, held for 2 h, and slowly cooled to 1000 °C over a period of 36 h. Once the furnace reached 1000 °C the FeAs was decanted from the single crystals using a centrifuge. The size of the resulting crystals can be as large as $1 \times 8 \times 12$ mm$^3$.

Elemental analysis was performed on samples from different batches using wavelength dispersive x-ray spectroscopy in the electron probe microanalyzer of a JEOL JXA-8200 Superprobe. We found the relative cobalt content $x = \text{Co}/(\text{Co}+\text{Fe}) \approx (7.4 \pm 0.2)\%$ so that we are dealing with

 

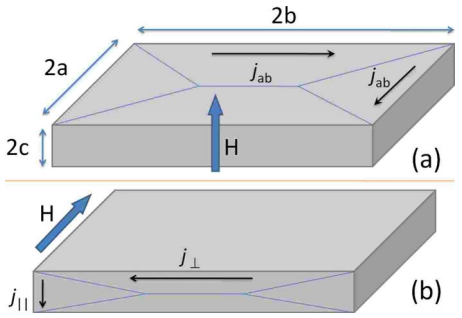


FIG. 1. (Color online) The samples are cuboids with the shortest side along the crystallographic $c$ axis. For the convenience of calculations sample dimensions are denoted as $2c \leq 2a \leq 2b$ with $a$ and $b$. The notation for the currents flowing in the critical state are shown for (a) $H \| c$ and (b) $H \| a$.

$Ba(Fe_{0.926}Co_{0.074})_2As_2$ (a rounded value of $x=0.07$ is used in the text). Furthermore, several samples from different batches showed a superconducting transition at $T_c \approx 22$ K, as determined from dc magnetization (an inset of Fig. 2) and from transport measurements, Fig. 9.

All studied samples were cuboid shaped with the crystallographic $c$ axis along the shortest dimension as shown schematically in Fig. 1. For convenience in calculations, we denote the sample dimensions as $2c \leq 2a \leq 2b$. The edges $a$ and $b$ lie in the crystallographic $ab$ plane, but do not necessarily correspond to the $a$ and $b$ axes. From all of our measurements and from the literature, no in-plane anisotropy of vortex properties have been reported and is not expected in a tetragonal system.

For the measurements reported here of the total magnetic moment (global magnetic measurements), a cuboid-shaped sample (see Fig. 3) of dimensions $0.28 \times 0.7 \times 1.26$ mm$^3$ was fixed in a gelatine capsule with a small amount of Apiezon grease. The capsule was placed in a clear plastic straw. To check for possible errors due to mechanical misalignment of the sample assembly, the key measurements [such as $M(H)$ loops] were repeated three times, each time after the sample was removed and reassembled. No noticeable variation in the results was found. Four samples from different batches were studied and they have all consistently shown the same behavior. The magnetization measurements were conducted in a *Quantum Design* MPMS magnetometer. The upper critical field, $H_{c2}(T)$, estimated from the onset of superconductivity, was measured by using a tunnel-diode resonator technique.[16]

Samples for transport measurements were cut into long thin bars having typical dimensions of $0.02 \times 0.1 \times (2-3)$ mm$^3$. Contacts were made by soldering silver wires with a silver-based alloy and had less than 0.1% of the sample resistance. Both two- and four-probe measurements were employed. To sustain a high current density without thermal shock, samples were glued with GE varnish onto an insulating heat sink substrate. Current wires were thermally anchored to two silver foil heat sinks (see inset in Fig. 8). Current-voltage characteristics were measured in a *Quantum Design* PPMS in the constant current mode. The highest obtainable current density was restricted to keep Joule heating to less than 1 K at $T_c$.

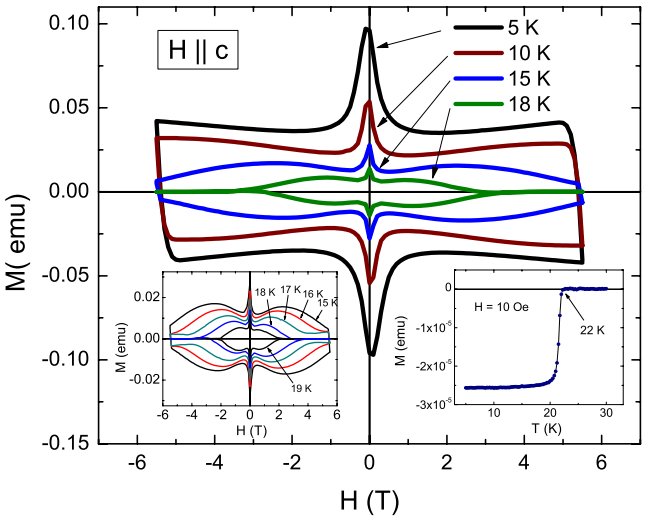


FIG. 2. (Color online) Magnetization loops measured in a $0.28 \times 0.7 \times 1.26$ mm$^3$ single crystal of $Ba(Fe_{0.93}Co_{0.07})_2As_2$ in a magnetic field $H \| c$ at $T=5$, 10, 15, and 18 K. The left inset zooms at the higher temperature region for $T=15$, 16, 17, 18, and 19 K where the evolution of the fishtail magnetization is clearly seen. The right inset shows a superconducting transition measured after zero-field cooling at $H=10$ Oe.

Magneto-optical (MO) imaging was performed in a $^4$He optical flow-type cryostat utilizing the Faraday rotation of polarized light in a Bi-doped iron-garnet indicator film with in-plane magnetization.[17] The spatial resolution of the technique is about 3 $\mu$m with a sensitivity to magnetic fields of about 1 G. The temporal resolution, as determined by our image acquisition hardware, is about 30 msec. In all images, the intensity is proportional to the local value of the magnetic induction perpendicular to the sample surface.

## III. RESULTS AND DISCUSSION

### A. Magnetization

In this section we present data on the irreversible magnetization in the mixed state of $Ba(Fe_{0.93}Co_{0.07})_2As_2$. One of the samples used, $0.28 \times 0.7 \times 1.26$ mm$^3$, is shown in the inset of Fig. 3. When the magnetic field is oriented along the $i$ edges ($i=a,b,c$) the measured magnetic moment per unit volume (the magnetization) is denoted as $M_i$. The currents in the system are determined by pinning properties, which in turn depend on orientations of the field and of the field gradients, i.e., of supercurrents. It is reasonable to assume that for $H \| c$, the currents $j_{ab}$ in the tetragonal crystals of interest here are isotropic in the $ab$ plane (see the upper panel of Fig. 1). If $H \| a$, the currents flow along $b$ and $c$ as shown in the lower panel of Fig. 1; it is worth noting that in this case $j_b \neq j_{ab}$ in the previous situation due to different orientation of vortices and of the gradients of their density. We, thus, denote the currents of this configuration as $j_\perp$ and $j_\parallel$ as shown in Fig. 1(b). Anisotropic current densities along with other anisotropic parameters will be reported elsewhere.[18]

Figure 2 shows $M(H)$ loops measured at several temperatures in magnetic fields $H \| c$. A noticeable nonmonotonic

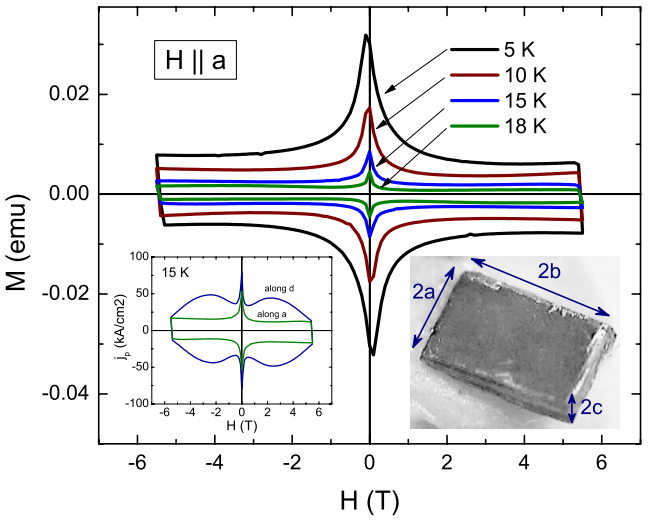


FIG. 3. (Color online) Magnetization loops for $H\|a$ in the $Ba(Fe_{0.93}Co_{0.07})_2As_2$ single crystal. The crystal is shown in the right inset and has dimensions $0.28\times0.7\times1.26$ mm$^3$. Left inset: comparison of $M(H)$ loops at $T=15$ K for two field orientations.

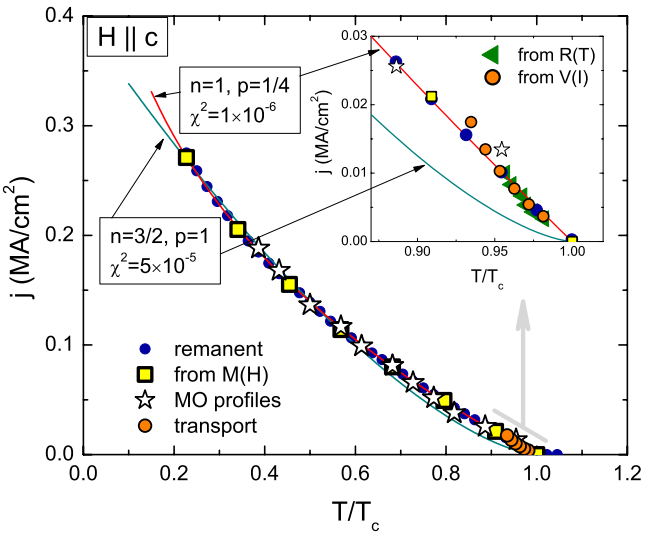


FIG. 4. (Color online) Supercurrent density in same-batch single crystals $Ba(Fe_{0.93}Co_{0.07})_2As_2$. "Magnetic" current density estimated from Eq. (1) at zero applied field by annealing of the remanent magnetization (filled circles) from $M(H)$ loops measured at different temperatures (squares), from magneto-optical profiles using Eq. (2) (stars), and from direct transport measurements (open circles). The lines show fits to $j(T)=j(0)[1-(T/T_c)^p]^n$ of the data set shown in full circles with indicated exponents and adjusted $\chi^2$ values. Inset zooms at the region of $T_c$ for easier comparison with the transport data obtained from Fig. 8 (circles) and Fig. 9 (triangles).

"fishtail" magnetization develops at elevated temperatures. Presumably, the fishtail exists also at the lower temperatures, but it is shifted to much higher fields beyond our reach. The left inset in Fig. 2 zooms into the high-temperature domain to show the details of the fishtail evolution with temperature. This behavior is remarkably similar to that of YBCO crystals.[19,20]

The situation is different when the field is applied along the $ab$ plane. Figure 3 shows the data for $H\|a$. No noticeable fishtail behavior is recorded in available fields even at high temperatures. The difference is clearly seen in the left inset, where the $M(H)$ loops at $T=15$ K for the two field orientations are shown. When the field was applied along the longer $b$ edge, the result (corrected for the difference in the cross sections perpendicular to the field) was essentially the same as for $H\|a$. Similar behavior of $M(H)$ for these two field orientations has been observed in several crystals with very different aspect ratios, which exclude possible geometric effects.

To determine the supercurrent in the critical state from magnetic measurements, we use the Bean model with field-independent supercurrent density.[21,22] For $H\|c$, the supercurrent density is given by

$$j_{ab}=\frac{10M_c}{a}\left(1-\frac{a}{3b}\right)^{-1}. \quad (1)$$

Equation (1) is written in practical units (based on cgs where the speed of light is $c=10$)[22] where length is in cm, volume magnetization $M$ is in emu/cm$^3$ (the *Quantum Design* MPMS reports the total measured moment in emu), and current density is in A/cm$^2$. It is assumed here that the reversible component of $M$ is small and can be ignored. [If not, one could extract the symmetric irreversible part by averaging the descending and ascending branches of the $M(H)$ loop.]

The supercurrent density $j_{ab}(T,H=0)$ extracted from the $M(H)$ measurements by using Eq. (1) is shown in Fig. 4 by open square symbols. An alternative and quicker way to determine the supercurrent density is by annealing of the trapped flux. With this approach, a full remanent state was induced at 5 K by cooling in a 5.5-T magnetic field and then turning the field off at 5 K. Then, this remanent state was slowly warmed up, allowing the temperature to stabilize before each measurement was taken. This convenient method is relatively quick and produces a curve with many data points. However, it must be justified whether we probe the original critical state relaxed only during the time window $\Delta t$, characteristic of our magnetometer, or the supercurrent has relaxed more and we are probing a deeply relaxed state. As can be seen in Fig. 4, the data obtained with the remanent annealing method (filled circles in Fig. 4) simply fall on top of the values obtained from the $M(H)$ loops (Fig. 4, open squares). The explanation is that the change in temperature occurs during a relatively short period of time, comparable to the time of setting and stabilizing the magnetic field in the superconducting magnet of the MPMS magnetometer during the field ramp.

Next we present somewhat unexpected results obtained in magnetic field. Using the annealing method described above for the remanent state, but this time annealing the induced critical state in finite fields (cooling in the highest field and then reducing it to a specified lower value at low temperature), we have obtained a set of $j(T)$ curves for different values of $H$. The result is shown in Fig. 5. There is an apparent pronounced decrease in the current density marked by open squares. Similarly, the temperature at which $j_{ab}\to0$ is marked by open circles. The latter feature is obviously the experimental irreversibility line, above which pinning is neg-

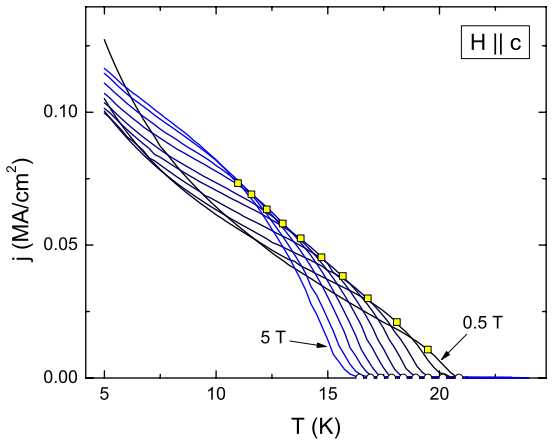


FIG. 5. (Color online) Supercurrents $j(T)$ measured in a single crystal $Ba(Fe_{0.93}Co_{0.07})_2As_2$ upon warming after 5.5-T field was reduced to the indicated values of the applied magnetic field at 5 K. Open circles mark the temperatures where $j \to 0$ (the irreversibility line above which the vortex lattice pinning vanishes). The squares mark the temperatures at which $j(T)$ curves exhibit a change in behavior (marking the fishtail feature as discussed below).

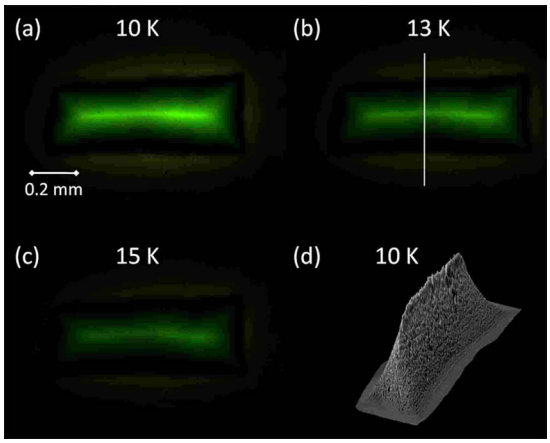


FIG. 6. (Color online) Magneto-optical images of a crystal $Ba(Fe_{0.93}Co_{0.07})_2As_2$ ($0.053 \times 0.24 \times 0.55$ mm$^3$) in the remanent state. The field was applied along the $c$ axis (perpendicular to the page) above $T_c$ and removed after cooling to 5 K. Frames (a), (b), and (c) show images for $T=10$, 13, and 15 K, respectively. Frame (d): a three-dimensional profile of the induction $B_z(x,y)$ perpendicular to the sample surface obtained from the data shown in (a).

ligible and the vortex liquid sets in. As for the former feature, we find that it coincides with the field, $H_p(T)$, at which a maximum in fishtail $M(H)$ loops is observed. Thus, the crossover in pinning (and relaxation) is seen in both magnetic-field- and temperature-dependent measurements of the supercurrent.

### B. Magneto-optical imaging

Another way to evaluate the supercurrent density is to examine the structure of the critical state by recording the spatial distribution of the magnetic induction $B$ on the sample surface. For this purpose the samples from the same batch as for $M(H)$ measurements have been used. The magneto-optical technique provides the component $B_z$ of the induction perpendicular to the sample surface.

The 1500 Oe magnetic field was applied along the $c$ axis above $T_c$ and *removed* after cooling to 5 K. The images obtained are shown in Fig. 6. Frames (a), (b), and (c) show the remanent state obtained at $T=10$, 13, and 15 K, respectively. Figure 6(d) is a three-dimensional plot of $B_z(x,y)$. The distorted oblique wedge shape of this profile is expected from the Bean critical state model for a thin sample.[21,22] The imaging also shows good homogeneity of the superconducting properties of the studied sample. We can, therefore, use the induction profiles to calculate the current density in the critical state. The $B(x)$ profiles, measured along the line shown in Fig. 6(b), are plotted in Fig. 7 for a few different temperatures. The profiles are typical for thin slablike samples. There is a clear neutral line where the field generated by the Bean supercurrents at the sample surface changes sign.

The maximum variation in the magnetic induction $\Delta B$ in the critical state (defined in Fig. 7) in a long sample with rectangular cross section has been calculated in Ref. 23,

$$\frac{5\Delta B}{2aj_{ab}} = \eta \ln \frac{(1+4\eta^2)^2}{16\eta^3\sqrt{1+\eta^2}} + 2\tan^{-1}2\eta - \tan^{-1}\eta, \qquad (2)$$

where $\eta = c/a$ and $B$ is measured in gauss and current density in A/cm$^2$. For the sample used in the MO study $\eta \approx 0.22$ and Eq. (2) yields $j_{ab} \approx 194\Delta B$. The currents calculated according to this formula are shown as stars in Fig. 4. Thus, both $M(H)$ loops and magneto-optical data produce practically the same estimate of the critical state currents.

### C. Transport measurements

Figure 8 shows current-voltage characteristics for a set of temperatures from 22.5 K down to 20.5 K. A photograph of the sample with the contacts is shown in the upper inset. Given the hardware and contact-imposed limitations, we

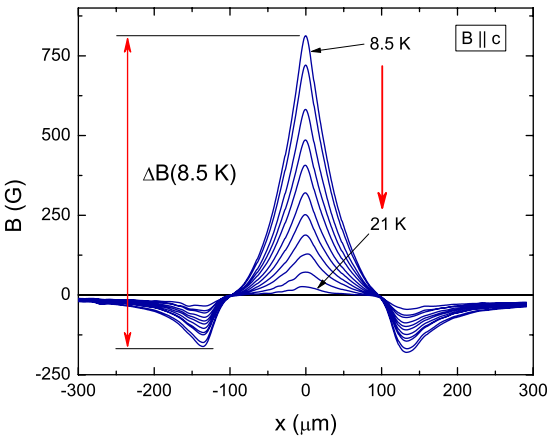


FIG. 7. (Color online) Profiles of the magnetic induction for a few different temperatures along the line shown in Fig. 6(b). Definition of the maximum variation in the magnetic induction, $\Delta B$, is shown for $T=8.5$ K.

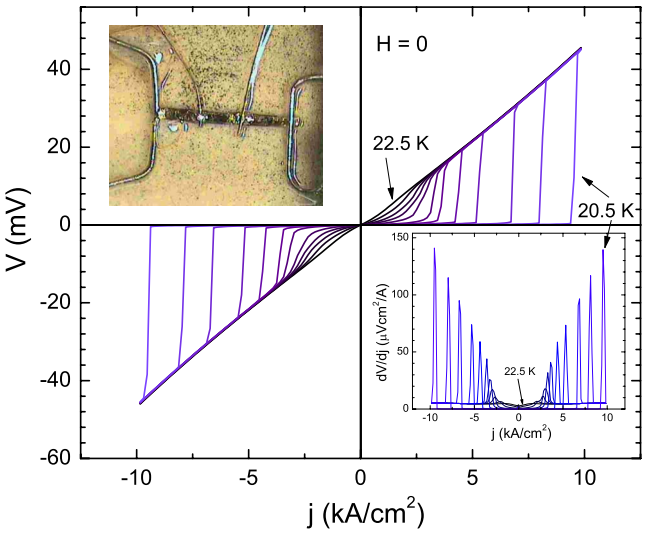


FIG. 8. (Color online) Zero-field current-voltage characteristics at indicated temperatures in a bar-shaped, $3\times0.1\times0.02$ mm$^3$, crystal of $Ba(Fe_{0.93}Co_{0.07})_2As_2$ with the current flowing in the *ab* plane. Upper inset: A photograph of the sample with contacts. Lower inset: The derivative $dV/dj$ used to identify the current $j$ which drives the system normal.

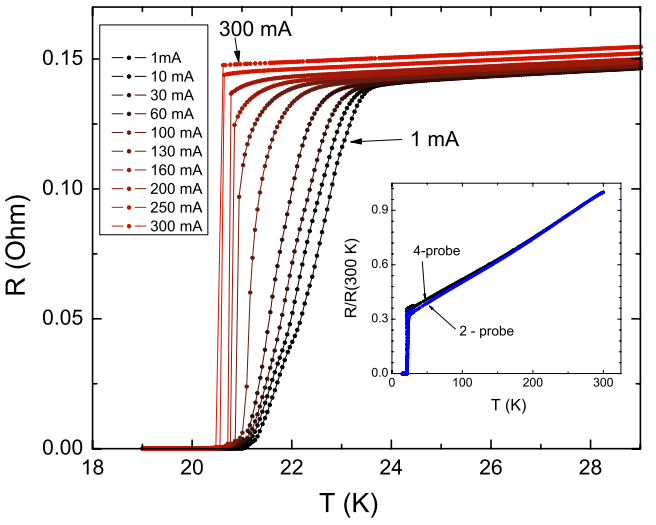


FIG. 9. (Color online) Resistance as a function of temperature for different dc transport currents in a $3\times0.1\times0.02$ mm$^3$ crystal. The onset of nonzero resistance was used to determine the temperature dependence of the maximum transport supercurrent density. Inset: normalized resistance in a full-temperature range measured by two- and four-probe methods.

could reach the current-induced transition to the normal state only in a narrow temperature interval near $T_c$. However, this was sufficient to overlap with the current values extracted from the $M(H)$ data. Sample dimensions were determined in a calibrated optical microscope and we estimate a 10% accuracy in the current density.

In the normal state, the curves $V(j)$ remain linear up to $j\approx10$ kA/cm$^2$. For higher currents, self-heating results in nonlinearity. We define the maximum transport current density $j_{tr}$, which causes a transition to the normal state as a position of an easily identifiable peak in the derivative $dV/dj$ (see Fig. 8). The resulting $j_{tr}(T)$ is shown in Fig. 4 (open circles—see inset).

In order to avoid the dynamic effect related to sweeping the current, we have estimated $j_{tr}$ also from the resistance onset in the curves $R(T)$ measured at different values of the current. These are shown in Fig. 4 by solid triangles. The resistance between current leads measured by a two-probe technique and in the conventional four-probe configuration is shown in the inset of Fig. 9 for the full-temperature range. The data scales perfectly with the sample geometry as the distance between contacts for the voltage readings are different.

The overall temperature dependences of the supercurrent density versus $T$ from different techniques are summarized in the main panel of Fig. 4. The inset in Fig. 4 compares the supercurrent obtained from magnetic measurements with direct transport measurements. There is good agreement between all data sets. We, therefore, conclude that, similar to $NdFeAsO_{1-x}F_x$,[1] the supercurrent density in single crystals of $Ba(Fe_{0.93}Co_{0.07})_2As_2$ is relatively low even at low temperatures, $j(T=5\ \mathrm{K},\ H=0)\simeq2.6\pm0.2\times10^5$ A/cm$^2$, which is comparable to Y-Ba-Cu-O single crystals. As for the functional form of $j_c(T)$, we can use the generalized power law that is usually used for superconductors, $j(T)=j(0)[1-(T/T_c)^p]^n$, which gives the best fit to the experimental data (most data points—solid symbols) with $j(0)\approx0.88$ MA/cm$^2$, $p=1/4$, and $p=1$. An attempt to fit with $p=1$ and $n=3/2$ is also shown in Fig. 4 and is inferior to the former fit, which is reflected in an order of magnitude larger adjusted $\chi^2$ value.

### D. Magnetic relaxation

The two major approaches to understand the fishtail behavior of the magnetization are the static and dynamic ones. The first is believed to work in alloys, ceramics, and materials with secondary phases.[24,25] In single crystals, however, the dynamic scenario related to the critical state relaxation and field-dependent flux creep is more plausible, as in the case of the high-$T_c$ cuprates.[26,27] For this reason, we examine the magnetic relaxation of the critical state as a function of temperature and magnetic field.

For the discussion below we should make the following distinction: The *true* critical current density $j_c$ marks the crossover between the regimes of flux flow and flux creep; at $j=j_c$ the current-dependent barrier $U(j/j_c)$ for the vortex escape from the pinning potential vanishes. The supercurrent density, $j$, which is recorded experimentally is always smaller than $j_c$. It is this supercurrent that determines the usefulness of a particular superconductor for current-carrying applications. This measured supercurrent is determined by the time window of the experiment $\Delta t$. It can be estimated from the logarithmic solution of the flux creep equation, $U(j/j_c)=T\ln(1+\Delta t/t_0)$.[28] Here, $U(j/j_c)$ is the barrier for thermal activation (in kelvin) and $t_0\sim10^{-5}-10^{-7}$ s is the *macroscopic* characteristic time that depends on the sample size and shape, as well as on the microscopic attempt time $\tau_0\sim10^{-10}-10^{-13}$ s.[27,29,30] There is a useful interpolation for-

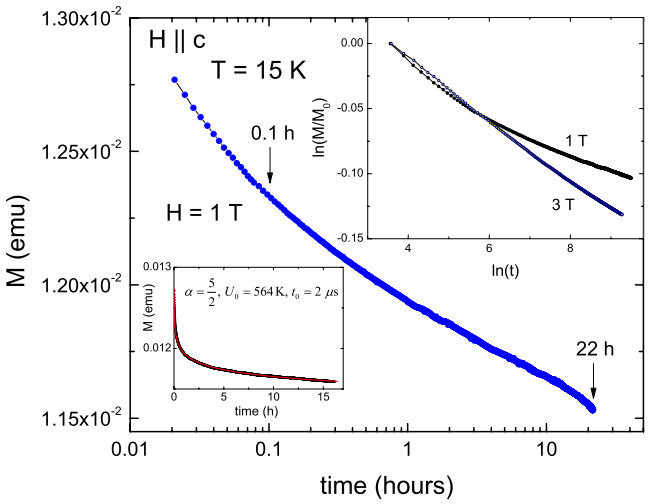


FIG. 10. (Color online) Time dependence of magnetization during 22 h at $T=15$ K with $H=1$ T after reducing magnetic field to zero from 5 T. Lower inset: fit to Eq. (4) with parameters indicated. Upper inset: ln-ln plot of $M(t)$ for $H=1$ and 3 T.

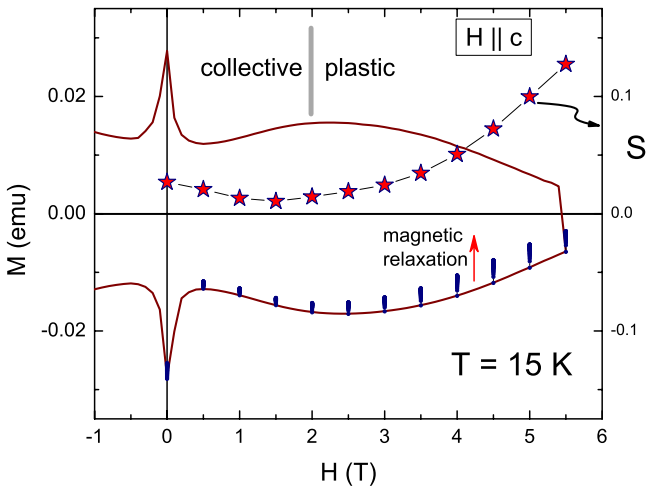


FIG. 11. (Color online) The field dependence of magnetization relaxation rate $S$ in a single crystal of $Ba(Fe_{0.93}Co_{0.07})_2As_2$ shown along with the $M(H)$ loop measured at the same temperature $T=15$ K.

mula for the creep barrier, which covers all known functional forms of $U(j/j_c)$,[31]

$$U(j) = \frac{U_0}{\alpha}\left[\left(\frac{j_c}{j}\right)^{\alpha} - 1\right]. \tag{3}$$

For $\alpha=-1$, Eq. (3) describes the Anderson-Kim barrier linear in $j/j_c$.[32,33] For $\alpha=-1/2$, the barrier for plastic creep driven by motion of the vortex lattice dislocations is obtained.[19] Positive $\alpha$ describes collective creep barriers.[30] In the limit $\alpha\to 0$, this formula reproduces the logarithmic barrier.[34] The activation energy of Eq. (3) results in a time-dependent magnetization of the form

$$M(t) = M_c\left(1 + \frac{\alpha T}{U_0}\ln\frac{t}{t_0}\right)^{-1/\alpha}. \tag{4}$$

For $\alpha=0$, a power-law decay is obtained, $M(t) = M_c(t_0/t)^{T/U_0}$. Generalization of the flux creep theory beyond the logarithmic solution with applications to the collective creep and the fishtail effects are given by in Ref. 27.

The flux creep is commonly characterized by the logarithmic relaxation rate $S=-|\mathrm{d}\ln M/\mathrm{d}\ln t|$. Equation (4) yields

$$S = \frac{T}{U_0}\left(1 + \frac{\alpha T}{U_0}\ln\frac{t}{t_0}\right)^{-1}. \tag{5}$$

We note that no single equation for relaxation is applicable for all values of $j/j_c$ and $H$. Within the collective creep theory, parameters $U_0$ and $\alpha$ depend on whether one deals with the creep of single vortices, of small or large vortex bundles.[30] The bundle regime changes as $j/j_c$ decreases. Therefore, the time dependence of the relaxing $M(t)$ will change. An example of our relaxation data for $H=1$ T is shown in Fig. 10. At longer times the (ln-ln) curvature starts to change. However, looking for the best fit to Eq. (4) in the widest possible time interval, we have determined that the small-bundle regime describes the data quite well as is shown in the lower inset. The fit parameters are reasonable within the collective creep model: for $\alpha=5/2$, $U_0\approx 564$ K, and $t_0\approx 2$ $\mu$s.

We now examine relaxation in magnetic fields above and below the peak position, $H_p(T)$, of the fishtail magnetization $M(H)$. To this end, we plot the $M(H)$ loop at 15 K and the relaxation rate $S(H)$ on the same graph, Fig. 11. For $H_p \approx 2.5$ T, we find different time dependencies $M(t)$ for $H < H_p$ and for $H > H_p$; an example is given in the upper inset of Fig. 10 for $H=1$ and 3 T. As is seen in Fig. 11, above $H_p$, the relaxation rate is faster than for $H<H_p$ and functional forms of $M(t)$ are different in these domains. Here, each $M(H=\mathrm{const},t)$ trace is plotted along with the regular magnetization loop.

The relaxation rate $S$ decreases marginally with time. For example, at 15 K and 1 T it drops only by a factor of 2.6 at the longest time of data collection (22 h). We estimate $S \approx 0.027$ at short times. This value is much larger than the rate for conventional superconductors, but is comparable to that of high-$T_c$ compounds.[26] We can say, therefore, that single crystals of $Ba(Fe_{0.93}Co_{0.07})_2As_2$ exhibit a "giant flux creep."[35]

We further observe that $S(H)$ (shown in Fig. 11) *decreases* with increasing $H$ approximately up to the field $H_p$, the position of the maximum of the fishtail $M(H)$ curve. This behavior is in agreement with the weak collective creep theory. However, above $H_p$, $S(H)$ *increases*, which contradicts this theory.

To clarify whether this behavior is related to the fishtail phenomenon, we have measured the magnetic relaxation rate with the field applied along the $a$ edge. In this case we do not observe the fishtail feature and the rate $S$ is monotonic (Fig. 12). We, therefore, conclude that the collective creep model fails above $H_p$.

Let us turn now to the temperature dependence of $S$. Figure 13 shows $S(T)$ measured in the zero-field remanent state for three orientations of the originally applied field. When vortices are parallel to the $ab$ plane, the relaxation rates are practically the same; for the relaxation of $M_c$, a similar $S(T)$ is shifted to slightly lower temperatures.

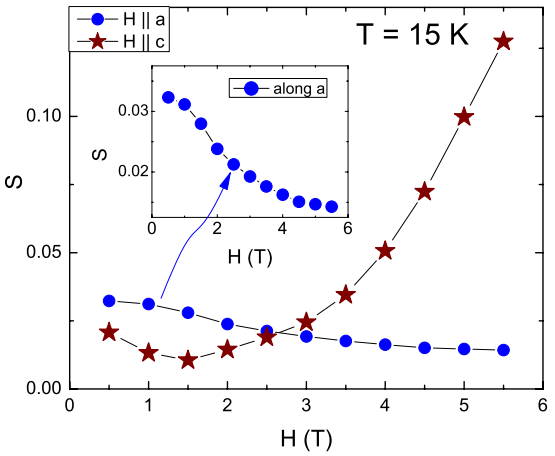


FIG. 12. (Color online) Comparison of the relaxation rate $S(H)$ for two field orientations at $T=15$ K.

The bell-shaped curves of $S(T)$ were observed in many superconductors with weak pinning, but to our knowledge no commonly accepted physical picture for such behavior is available. Formally, one can assume that the exponent $\alpha$ in Eq. (5) is temperature dependent. It follows from the collective creep theory that $\alpha$ is nonmonotonic with respect to the bundle size.[30] The latter might be $T$ dependent, thus, resulting in a desirable $S(T)$. Thus, the bell-shaped $S(T)$ in zero-field can, in principle, be understood within the collective creep theory.

Using similar arguments, one can show that the plastic creep can only lead to a monotonic increase in the relaxation rate on warming.[19] Our data show that, in contrast to the case of the zero-field remanent field, the relaxation rate of $M_c$ in a fixed field above $H_p$ (shown in Fig. 13) is an order of magnitude larger than for $H=0$ and increases on warming.

The idea of the plastic vortex creep as responsible for this behavior has been introduced when a similar failure of the collective creep model was found[19] in single crystals of YBCO and of the electron-doped $Nd_{0.85}Ce_{0.15}CuO_{4-x}$.[36] The

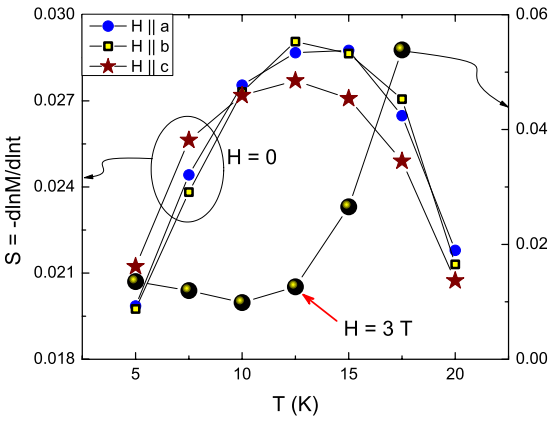


FIG. 13. (Color online) Logarithmic relaxation rate as a function of temperature measured in a single crystal of $Ba(Fe_{0.93}Co_{0.07})_2As_2$ in the remanent state, $H=0$, in three orientations of the trapped vortex direction with respect to the sample. For comparison, $S(T)$ at $H=3$ T is shown. (Note different origins and scales of the left and right axes).

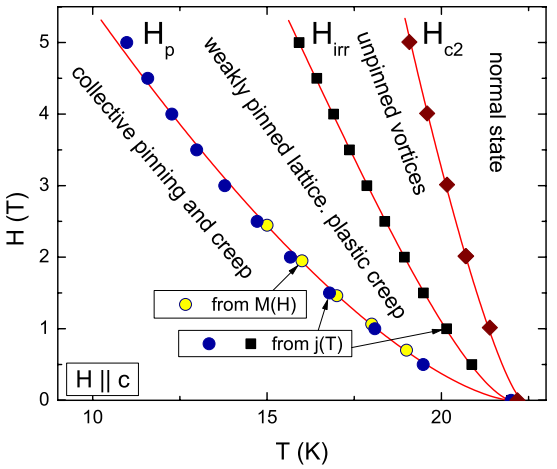


FIG. 14. (Color online) The $H$-$T$ phase diagram of $Ba(Fe_{0.93}Co_{0.07})_2As_2$ single crystals in the mixed state. The solid lines are fits to the commonly used form $H_{xx}(T)=H_{xx}(0)[1-(T/T_c)^p]^n$. We obtained for the fishtail peak position $H_p(0)\approx 13.6$ T, $n=3/2$, and $p=1$. For the irreversibility line: $H_{irr}(0)\approx 15.2$ T, $n=3/2$, and $p=2$. For the upper critical field: $H_{c2}(0)\approx 66.7$ T, $n=4/3$, and $p=1$.

measured $V(j)$ characteristics have confirmed the plastic creep model.[37] These and later works have shown that in crystals with moderate pinning, a crossover from elastic to plastic creep is always accompanied by the fishtail shape of $M(H)$. Still, it should be noted that the fishtail feature itself is due to peculiarities of the collective creep when the relaxation rate is faster for smaller magnetic fields. Within the plastic scenario, the thermally activated creep is not due to jumps of vortex bundles, but to sliding of dislocations in the vortex lattice. Unlike the collective creep model, the barrier for magnetic relaxation within this approach, $U_{pl}(B,j/j_c)=U_{pl}(B)(1-\sqrt{j/j_c})$, remains finite as $j\to 0$. It decreases with increasing magnetic field, $U_{pl}(B)\sim 1/\sqrt{B}$, because the elementary steps of a dislocation are proportional to the intervortex distance.

On the other hand, the collective creep barriers increase with magnetic field as $U_c(B)\sim B^{\nu}$, where $\nu$ is positive and depends on particularities of the pinning regime. The $j$ dependence of $U$ is given by Eq. (3) with positive $\alpha$ that gives in a diverging barrier $U\sim(j_c/j)^{\alpha}$. In low fields, the collective barrier is smaller than the plastic one, and therefore, the collective channel dominates the vortex dynamics. However, as the field increases, the crossover from the collective to plastic channel of vortex relaxation occurs when $U_{pl}(B,j/j_c)$ becomes smaller than $U_{col}(B,j/j_c)$.

## IV. SUMMARY

Finally, Fig. 14 presents the phase diagram of $Ba(Fe_{0.93}Co_{0.07})_2As_2$ single crystals in the mixed state compiled from our results. It closely resembles diagrams for the cuprate superconductors, in particular of YBCO and NCCO single crystals. The prominent features are the irreversibility line that is quite distant from the $H_{c2}(T)$ curve and a clear crossover line between collective and plastic creep regimes.

Together with Fig. 4 for the supercurrent density this summarizes our findings.

In conclusion, detailed measurements of global and local electromagnetic properties show that the vortex behavior in single-crystalline superconducting $Ba(Fe_{0.93}Co_{0.07})_2As_2$ is similar to that found in the high-$T_c$ cuprates. In particular, we report the presence of a fishtail feature in $M(H,T=\text{const})$ loops and find its signature in $M(H=\text{const},T)$ measurements. Furthermore, magnetic relaxation measurements are consistent with the collective pinning and creep models (weak pinning and fast creep) and suggest a crossover to the plastic creep regime in fields exceeding $H_p$, the position of the maximum in the fishtail magnetization. It is known that zero-field anisotropy of the magnetic properties in the superconducting state of $Ba(Fe_{0.93}Co_{0.07})_2As_2$ is small, between 2 and 4 (Ref. 18) for the upper critical field, normal-state resistivity, and London penetration depth. Vortex behavior, however, changes for different orientations of magnetic field with respect the crystal axes as shown in the present work. This implies field-dependent anisotropy of at least pinning properties and maybe also other parameters of the superconducting state.

## ACKNOWLEDGMENTS

We thank J. Clem, A. Koshelev, R. Mints, and J. Schmalian for helpful discussions. Work at the Ames Laboratory was supported by the U.S. Department of Energy-Basic Energy Sciences under Contract No. DE-AC02-07CH11358. R.P. acknowledges support from Alfred P. Sloan Foundation.

*Corresponding author: prozorov@ameslab.gov

[1] R. Prozorov, M. E. Tillman, E. D. Mun, and P. C. Canfield, arXiv:0805.2783 (unpublished).
[2] A. Yamamoto, J. Jiang, C. Tarantini, N. Craig, A. A. Polyanskii, F. Kametani, F. Hunte, J. Jaroszynski, E. E. Hellstrom, D. C. Larbalestier, R. Jin, A. S. Sefat, M. A. McGuire, B. C. Sales, D. K. Christen, and D. Mandrus, Appl. Phys. Lett. **92**, 252501 (2008).
[3] J. Jaroszynski, S. C. Riggs, F. Hunte, A. Gurevich, D. C. Larbalestier, G. S. Boebinger, F. F. Balakirev, A. Migliori, Z. A. Ren, W. Lu, J. Yang, X. L. Shen, X. L. Dong, Z. X. Zhao, R. Jin, A. S. Sefat, M. A. McGuire, B. C. Sales, D. K. Christen, and D. Mandrus, Phys. Rev. B **78**, 064511 (2008).
[4] Y. L. Chen, Y. J. Cui, Y. Yang, Y. Zhang, L. Wang, C. H. Cheng, C. Sorrell, and Y. Zhao, Supercond. Sci. Technol. **21**, 115014 (2008).
[5] S. Weyeneth, U. Mosele, N. D. Zhigadlo, S. Katrych, Z. Bukowski, J. Karpinski, S. Kohout, J. Roos, and H. Keller, arXiv:0806.1024 (unpublished).
[6] L. Balicas, A. Gurevich, Y. Jo, J. Jaroszynski, D. Larbalestier, R. Liu, H. Chen, X. Chen, N. Zhigadlo, S. Katrych, Z. Bukowski, and J. Karpinski, arXiv:0809.4223 (unpublished).
[7] N. Ni, S. L. Bud'ko, A. Kreyssig, S. Nandi, G. E. Rustan, A. I. Goldman, S. Gupta, J. D. Corbett, A. Kracher, and P. C. Canfield, Phys. Rev. B **78**, 014507 (2008).
[8] J.-Q. Yan, A. Kreyssig, S. Nandi, N. Ni, S. L. Bud'ko, A. Kracher, R. J. McQueeney, R. W. McCallum, T. A. Lograsso, A. I. Goldman, and P. C. Canfield, Phys. Rev. B **78**, 024516 (2008).
[9] N. Ni, S. Nandi, A. Kreyssig, A. I. Goldman, E. D. Mun, S. L. Bud'ko, and P. C. Canfield, Phys. Rev. B **78**, 014523 (2008).
[10] Z.-S. Wang, H.-Q. Luo, C. Ren, and H.-H. Wen, Phys. Rev. B **78**, 140501(R) (2008).
[11] A. S. Sefat, R. Jin, M. A. McGuire, B. C. Sales, D. J. Singh, and D. Mandrus, Phys. Rev. Lett. **101**, 117004 (2008).
[12] H. Yang, H. Luo, Z. Wang, and H.-H. Wen, Appl. Phys. Lett. **93**, 142506 (2008).
[13] A. Yamamoto, J. Jaroszynski, C. Tarantini, L. Balicas, J. Jiang, A. Gurevich, and D. Larbalestier, arXiv:0810.0699 (unpublished).
[14] N. Ni, M. E. Tillman, J.-Q. Yan, A. Kracher, S. T. Hannahs, S. L. Bud'ko, and P. C. Canfield, arXiv:0811.1767 (unpublished).
[15] R. T. Gordon, N. Ni, C. Martin, M. A. Tanatar, M. D. Vannette, H. Kim, G. Samolyuk, J. Schmalian, S. Nandi, A. Kreyssig, A. I. Goldman, J. Q. Yan, S. L. Bud'ko, P. C. Canfield, and R. Prozorov, arXiv:0810.2295 (unpublished).
[16] C. Martin, R. T. Gordon, M. A. Tanatar, M. D. Vannette, M. E. Tillman, E. D. Mun, P. C. Canfield, V. G. Kogan, G. D. Samolyuk, J. Schmalian, and R. Prozorov, arXiv:0807.0876 (unpublished).
[17] R. Prozorov, Phys. Rev. Lett. **98**, 257001 (2007).
[18] M. A. Tanatar, N. Ni, C. Martin, R. T. Gordon, H. Kim, V. G. Kogan, G. D. Samolyuk, S. L. Bud'ko, P. C. Canfield, and R. Prozorov (unpublished).
[19] Y. Abulafia, A. Shaulov, Y. Wolfus, R. Prozorov, L. Burlachkov, Y. Yeshurun, D. Majer, E. Zeldov, H. Wuhl, V. B. Geshkenbein, and V. M. Vinokur, Phys. Rev. Lett. **77**, 1596 (1996).
[20] P. D. Panetta, J. E. Ostenson, D. K. Finnemore, and C. L. Snead, Phys. Rev. B **52**, 15570 (1995).
[21] C. P. Bean, Phys. Rev. Lett. **8**, 250 (1962).
[22] C. P. Bean, Rev. Mod. Phys. **36**, 31 (1964).
[23] R. Prozorov, Ph.D. thesis, Bar-Ilan University, 1998; available at arXiv:0811.0177 (unpublished).
[24] W. DeSorbo, Rev. Mod. Phys. **36**, 90 (1964).
[25] A. M. Campbell and J. E. Evetts, *Critical Currents in Superconductors*, Monographs on Physics (Taylor & Francis, London, 1972).
[26] Y. Yeshurun, A. P. Malozemoff, and A. Shaulov, Rev. Mod. Phys. **68**, 911 (1996).
[27] L. Burlachkov, D. Giller, and R. Prozorov, Phys. Rev. B **58**, 15067 (1998).
[28] V. B. Geshkenbein and A. I. Larkin, Zh. Eksp. Teor. Fiz. **95**, 1108 (1989).
[29] A. Gurevich and H. Kupfer, Phys. Rev. B **48**, 6477 (1993).
[30] G. Blatter, M. V. Feigelman, V. B. Geshkenbein, A. I. Larkin, and V. M. Vinokur, Rev. Mod. Phys. **66**, 1125 (1994).
[31] R. Griessen, A. F. T. Hoekstra, H. H. Wen, G. Doornbos, and H. G. Schnack, Physica C **282-287**, 347 (1997).
[32] P. W. Anderson, Phys. Rev. Lett. **9**, 309 (1962).

[33] P. W. Anderson and Y. B. Kim, Rev. Mod. Phys. **36**, 39 (1964).
[34] E. Zeldov, N. M. Amer, G. Koren, A. Gupta, R. J. Gambino, and M. W. McElfresh, Phys. Rev. Lett. **62**, 3093 (1989).
[35] Y. Yeshurun and A. P. Malozemoff, Phys. Rev. Lett. **60**, 2202 (1988).
[36] D. Giller, A. Shaulov, R. Prozorov, Y. Abulafia, Y. Wolfus, L. Burlachkov, Y. Yeshurun, E. Zeldov, V. M. Vinokur, J. L. Peng, and R. L. Greene, Phys. Rev. Lett. **79**, 2542 (1997).
[37] D. Giller, Y. Abulafia, R. Prozorov, Y. Wolfus, A. Shaulov, and Y. Yeshurun, Phys. Rev. B **57**, R14080 (1998).